Structural and Magnetic Phase Transitions near Optimal Superconductivity in BaFe$_2$(As$_{1-x}$P$_x$)$_2$

Ding Hu,[1] Xingye Lu,[1] Wenliang Zhang,[1] Huiqian Luo,[1] Shiliang Li,[1,2] Peipei Wang,[1] Genfu Chen,[1,*] Fei Han,[3]
Shree R. Banjara,[4,5] A. Sapkota,[4,5] A. Kreyssig,[4,5] A. I. Goldman,[4,5] Z. Yamani,[6] Christof Niedermayer,[7]
Markos Skoulatos,[7] Robert Georgii,[8] T. Keller,[9,10] Pengshuai Wang,[11] Weiqiang Yu,[11] and Pengcheng Dai[12,1,†]

[1]*Institute of Physics, Chinese Academy of Sciences, Beijing 100190, China*
[2]*Collaborative Innovation Center of Quantum Matter, Beijing, China*
[3]*Materials Science Division, Argonne National Laboratory, Argonne, Illinois 60439, USA*
[4]*Ames Laboratory, U.S. DOE, Ames, Iowa 50011, USA*
[5]*Department of Physics and Astronomy, Iowa State University, Ames, Iowa 50011, USA*
[6]*Canadian Neutron Beam Centre, National Research Council, Chalk River, Ontario K0J 1P0, Canada*
[7]*Laboratory for Neutron Scattering, Paul Scherrer Institut, CH-5232 Villigen, Switzerland*
[8]*Heinz Maier-Leibnitz Zentrum, Technische Universität München, D-85748 Garching, Germany*
[9]*Max-Planck-Institut für Festkörperforschung, Heisenbergstrasse 1, D-70569 Stuttgart, Germany*
[10]*Max Planck Society Outstation at the Forschungsneutronenquelle Heinz Maier-Leibnitz (MLZ), D-85747 Garching, Germany*
[11]*Department of Physics, Renmin University of China, Beijing 100872, China*
[12]*Department of Physics and Astronomy, Rice University, Houston, Texas 77005, USA*
(Received 22 December 2014; published 17 April 2015)

We use nuclear magnetic resonance (NMR), high-resolution x-ray, and neutron scattering studies to study structural and magnetic phase transitions in phosphorus-doped BaFe$_2$(As$_{1-x}$P$_x$)$_2$. Previous transport, NMR, specific heat, and magnetic penetration depth measurements have provided compelling evidence for the presence of a quantum critical point (QCP) near optimal superconductivity at $x = 0.3$. However, we show that the tetragonal-to-orthorhombic structural (T_s) and paramagnetic to antiferromagnetic (AF, T_N) transitions in BaFe$_2$(As$_{1-x}$P$_x$)$_2$ are always coupled and approach $T_N \approx T_s \geq T_c$ ($\approx$29 K) for $x = 0.29$ before vanishing abruptly for $x \geq 0.3$. These results suggest that AF order in BaFe$_2$(As$_{1-x}$P$_x$)$_2$ disappears in a weakly first-order fashion near optimal superconductivity, much like the electron-doped iron pnictides with an avoided QCP.

A determination of the structural and magnetic phase diagrams in different classes of iron pnictide superconductors will form the basis from which a microscopic theory of superconductivity can be established [1–5]. The parent compound of iron pnictide superconductors such as BaFe$_2$As$_2$ exhibits a tetragonal-to-orthorhombic structural transition at temperature T_s and then orders antiferromagnetically below T_N with a collinear antiferromagnetic (AF) structure [Fig. 1(a)] [3,4]. Upon hole doping via partially replacing Ba by K or Na [6,7], the structural and magnetic phase transition temperatures in Ba$_{1-x}$A$_x$Fe$_2$As$_2$ (A = K, Na) decrease simultaneously with increasing x and form a small pocket of a magnetic tetragonal phase with the c-axis-aligned moment before disappearing abruptly near optimal superconductivity [8–11]. For electron-doped Ba(Fe$_{1-x}$T$_x$)$_2$As$_2$ (T = Co, Ni), transport [12,13], muon spin relaxation [14], nuclear magnetic resonance (NMR) [15–17], x-ray, and neutron scattering experiments [18–23] have revealed that the structural and magnetic phase transition temperatures decrease and separate with increasing x [18–23]. However, instead of a gradual suppression to zero temperature near optimal superconductivity as expected for a magnetic quantum critical point (QCP)

[15,16], the AF order for Ba(Fe$_{1-x}$T$_x$)$_2$As$_2$ near optimal superconductivity actually occurs around 30 K ($> T_c$) and forms a short-range incommensurate magnetic phase that competes with superconductivity and disappears in the weakly first-order fashion, thus avoiding the expected magnetic QCP [20–23].

Although a QCP may be avoided in electron-doped Ba(Fe$_{1-x}$T$_x$)$_2$As$_2$ due to disorder and impurity scattering in the FeAs plane induced by Co and Ni substitution, phosphorus-doped BaFe$_2$(As$_{1-x}$P$_x$)$_2$ provides an alternative system to achieve a QCP since substitution of As by the isovalent P suppresses the static AF order and induces superconductivity without appreciable impurity scattering [24–27]. Indeed, experimental evidence for the presence of a QCP at $x = 0.3$ in BaFe$_2$(As$_{1-x}$P$_x$)$_2$ has been mounting, including the linear temperature dependence of the resistivity [28], an increase in the effective electron mass seen from the de Haas-van Alphen effect [26], magnetic penetration depth [29,30], heat capacity [31], and normal state transport measurements in samples where superconductivity has been suppressed by a magnetic field [32]. Although these results, as well as NMR measurements [33], indicate a QCP originating from the suppression of the static AF
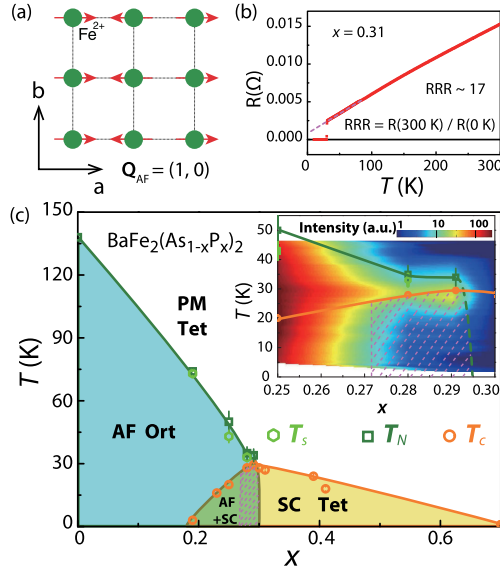
FIG. 1 (color online). (a) The AF-ordered phase of $BaFe_2(As_{1-x}P_x)_2$, where the magnetic Bragg peaks occur at $\mathbf{Q}_{AF} = (1, 0, L)$ $(L = 1, 3, \ldots)$ positions. (b) Temperature dependence of the resistance for the $x = 0.31$ sample, where $RRR = R(300\ K)/R(0\ K) \sim 17$. In previous work on similar P-doped samples, $RRR \sim 13$ [28]. (c) The phase diagram of $BaFe_2(As_{1-x}P_x)_2$, where the Ort, Tet, and SC are orthorhombic, tetragonal, and superconductivity phases, respectively. The inset shows the expanded view of the P-concentration dependence of T_s, T_N, and, T_c near optimal superconductivity. The color bar represents the temperature and doping dependence of the normalized magnetic Bragg peak intensity. The dashed region indicates the mesoscopic coexisting AF and SC phases.

order near $x = 0.3$, recent neutron powder diffraction experiments directly measuring T_s and T_N in $BaFe_2(As_{1-x}P_x)_2$ as a function of x suggest that structural quantum criticality cannot exist at compositions higher than $x = 0.28$ [34]. Furthermore, the structural and magnetic phase transitions at all studied P-doping levels are first order and occur simultaneously within the sensitivity of the measurements (~ 0.5 K), thus casting doubt on the presence of a QCP [34]. While these results are interesting, they were carried out on powder samples and, thus, are not sensitive enough to the weak structural or magnetic order to allow a conclusive determination on the nature of the structural and AF phase transitions near optimal superconductivity.

In this Letter, we report systematic transport, NMR, x-ray, and neutron scattering studies of $BaFe_2(As_{1-x}P_x)_2$ single crystals focused on determining the P-doping evolution of the structural and magnetic phase transitions near $x = 0.3$. While our data for $x \leq 0.25$ are consistent with the earlier results obtained from powder samples [34], we find that nearly simultaneous structural and magnetic transitions in single crystals of $BaFe_2(As_{1-x}P_x)_2$ occur at $T_s \approx T_N \geq T_c = 29$ K for $x = 0.28$ and 0.29 (near optimal doping) and disappear suddenly at $x \geq 0.3$. While superconductivity dramatically suppresses the static

AF order and lattice orthorhombicity below T_c for $x = 0.28$ and 0.29, the collinear static AF order persists in the superconducting state. Our neutron spin echo and NMR measurements on the $x = 0.29$ sample reveal that only part of the sample is magnetically ordered, suggesting its mesoscopic coexistence with superconductivity. Therefore, despite reduced impurity scattering, P-doped $BaFe_2As_2$ has remarkable similarities in the phase diagram to that of electron-doped $Ba(Fe_{1-x}T_x)_2As_2$ iron pnictides with an avoided QCP.

We have carried out systematic neutron scattering experiments on $BaFe_2(As_{1-x}P_x)_2$ with $x = 0.19, 0.25, 0.28, 0.29, 0.30$, and 0.31 [35] using the C5, RITA-II, and MIRA triple-axis spectrometers at the Canadian Neutron Beam center, Paul Scherrer Institute, and Heinz Maier-Leibnitz Zentrum (MLZ), respectively. We have also carried out neutron resonance spin echo (NRSE) measurements on the $x = 0.29$ sample using TRISP triple-axis spectrometer at MLZ [36]. Finally, we have performed high-resolution x-ray diffraction experiments on identical samples at Ames Laboratory and Advanced Photon Source (APS), Argonne National Laboratory (ANL) (see the Supplemental Material [37]). Our single crystals were grown using a Ba_2As_2/Ba_2P_3 self-flux method, and the chemical compositions are determined by inductively coupled plasma analysis with 1% accuracy [35]. We define the wave vector $\mathbf{Q}$ at (q_x, q_y, q_z) as $(H, K, L) = (q_x a/2\pi, q_y b/2\pi, q_z c/2\pi)$ reciprocal lattice units using the orthorhombic unit cell suitable for the AF-ordered phase of iron pnictides, where $a \approx b \approx 5.6$ Å and $c = 12.9$ Å. Figure 1(b) shows temperature dependence of the resistivity for $x = 0.31$ sample, confirming the high quality of our single crystals [28].

Figure 1(c) summarizes the phase diagram of $BaFe_2(As_{1-x}P_x)_2$ as determined from our experiments. Similar to previous findings on powder samples with $x \leq 0.25$ [34], we find that the structural and AF phase transitions for single crystals of $x = 0.19, 0.28$, and 0.29 occur simultaneously within the sensitivity of our measurements (~ 1 K). On approaching optimal superconductivity as $x \to 0.3$, the structural and magnetic phase transition temperatures are suppressed to $T_s \approx T_N \approx 30$ K for $x = 0.28, 0.29$ and then vanish suddenly for $x = 0.3, 0.31$ as shown in the inset of Fig. 1(c). Although superconductivity dramatically suppresses the lattice orthorhombicity and static AF order in $x = 0.28, 0.29$, there is still remnant static AF order at temperatures well below T_c. However, we find no evidence of static AF order and lattice orthorhombicity for $x = 0.3$ and 0.31 at all temperatures. Since our NMR measurements on the $x = 0.29$ sample suggest that the magnetic order takes place in about $\sim 50\%$ of the volume fraction, the coupled T_s and T_N AF phase in $BaFe_2(As_{1-x}P_x)_2$ becomes a homogeneous superconducting phase in the weakly first-order fashion, separated by a phase with coexisting AF clusters and superconductivity [dashed region in Fig. 1(c)].
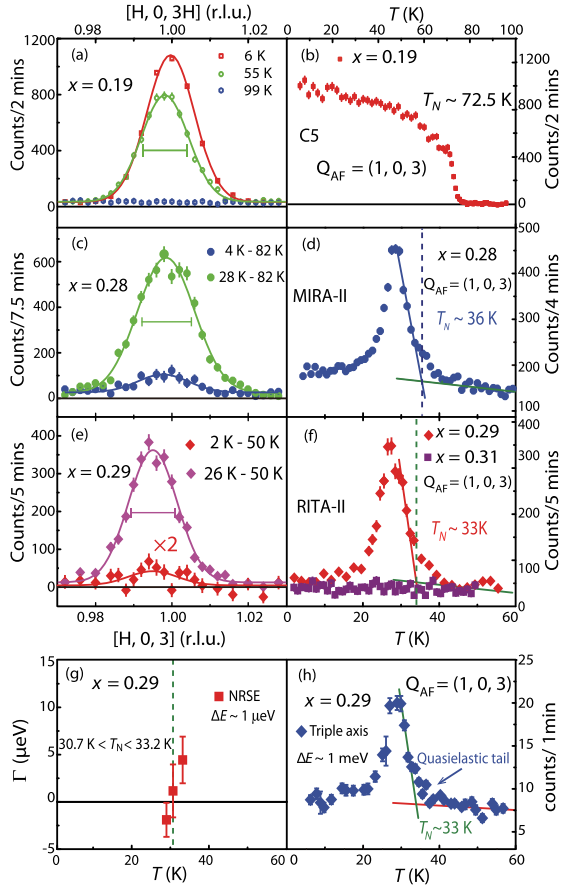
FIG. 2 (color online). [(a),(c),(e)] Wave vector scans along the $[H, 0, 3]$ direction at different temperatures for $x = 0.19, 0.28, 0.29$, and 0.31, respectively. Horizontal bars indicate instrumental resolution. [(b),(d),(f)] Temperature dependence of the magnetic scattering at $Q_{AF} = (1, 0, 3)$ for $x = 0.19, 0.28$, and 0.29, respectively. (g) NRSE measurement of temperature dependence of the energy width (Γ is the full-width-at-half-maximum (FHWM) of scattering function and 0 indicates instrumental resolution limited) at $Q_{AF} = (1, 0, 3)$ for $x = 0.29$. (h) The magnetic order parameters from the normal triple-axis measurement on the same sample.

To establish the phase diagram in Fig. 1(c), we first present neutron scattering data aimed at determining the Néel temperatures of $BaFe_2(As_{1-x}P_x)_2$. Figure 2(a) shows scans along the $[H, 0, 3H]$ direction at different temperatures for the $x = 0.19$ sample. The instrumental resolution limited peak centered at $Q_{AF} = (1, 0, 3)$ disappears at 99 K above T_N [Fig. 2(a)]. Figure 2(b) shows the temperature dependence of the scattering at $Q_{AF} = (1, 0, 3)$, which reveals a rather sudden change at $T_N = 72.5 \pm 1$ K consistent with the first-order nature of the magnetic transition [34]. Figure 2(c) plots $[H, 0, 0]$ scans through the (1,0,3) Bragg peak showing the temperature differences between 28 K (4 K) and 82 K for the $x = 0.28$ sample. There is a clear resolution-limited peak centered at (1,0,3) at 28 K indicative of the static AF order, and the scattering is suppressed but not eliminated at 4 K. Figure 2(d) shows the

temperature dependence of the scattering at (1,0,3), revealing a continuously increasing magnetic order parameter near T_N and a dramatic suppression of the magnetic intensity below T_c. Figures 2(e) and 2(f) indicate that the magnetic order in the $x = 0.29$ sample behaves similar to that of the $x = 0.28$ crystal without much reduction in T_N. On increasing the doping levels to $x = 0.3$ (Supplemental Material [37]) and 0.31 [Fig. 2(f)], we find no evidence of magnetic order above 2 K. Given that the magnetic order parameters near T_N for the $x = 0.28, 0.29$ samples look remarkably like those of the spin cluster phase in electron-doped $Ba(Fe_{1-x}T_x)_2As_2$ near optimal superconductivity [22,23], we have carried out additional neutron scattering measurements on the $x = 0.29$ sample using TRISP, which can operate as a normal thermal triple-axis spectrometer with instrumental energy resolution of $\Delta E \approx 1$ meV and a NRSE triple-axis spectrometer with $\Delta E \approx 1\ \mu$eV [36]. Figure 2(h) shows the triple-axis mode data which reproduce the results in Fig. 2(f). However, identical measurements using NRSE mode reveal that the magnetic scattering above 30.7 K is quasielastic and the spins of the system freeze below 30.7 K on a time scale of $\tau \sim \hbar/\Delta E \approx 6.6 \times 10^{-10}$ s [23]. This spin freezing temperature is almost identical to those of nearly optimally electron-doped $Ba(Fe_{1-x}T_x)_2As_2$ [21–23].

Figure 3 summarizes the key results of our x-ray scattering measurements carried out on samples identical to those used for neutron scattering experiments. To facilitate quantitative comparison with the results on $Ba(Fe_{1-x}T_x)_2As_2$, we define the lattice orthorhombicity $\delta = (a - b)/(a + b)$ [19,22]. Figure 3(a) shows the temperature dependence of δ for $BaFe_2(As_{1-x}P_x)_2$ with
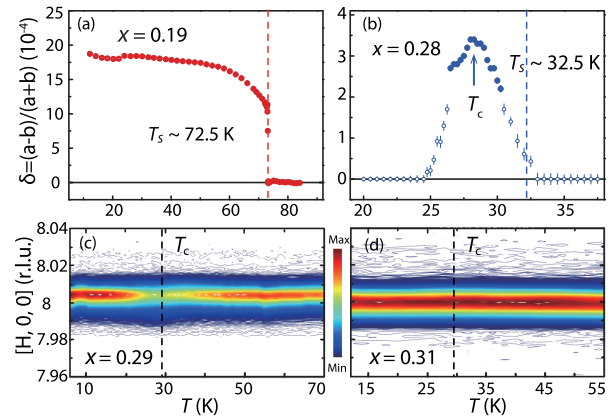

FIG. 3 (color online). Temperature evolution of δ for (a) $x = 0.19$ and (b) $x = 0.28$ samples. The solid circles indicate x-ray data where clear orthorhombic lattice distortions are seen. The open circles are data where one can only see peak broadening due to orthorhombic lattice distortion. Temperature dependence of the $[H, 0, 0]$ scans for (c) $x = 0.29$ and (d) $x = 0.31$. The vertical color bar indicates x-ray scattering intensity. The data were collected while warming the system from base temperature to a temperature well above T_s.

$x = 0.19$, obtained by fitting the two Gaussian peaks in longitudinal scans along the (8,0,0) nuclear Bragg peak (Supplemental Material [37]). We find that the lattice orthorhombicity δ exhibits a first-order-like jump below $T_s = 72.5$ K consistent with previous neutron scattering results [34,37]. We also note that the lattice distortion value of $\delta \approx 17 \times 10^{-4}$ is similar to those of $Ba(Fe_{1-x}T_x)_2As_2$ with $T_s \approx 70$ K [19,22].

Figure 3(b) shows the temperature dependence of δ estimated for the $x = 0.28$ sample. In contrast to the $x = 0.19$ sample, we only find clear evidence of lattice orthorhombicity in the temperature region of $26 \leq T \leq 32.5$ K [filled circles in Fig. 3(b)] (Supplemental Material [37]). The open symbols represent δ estimated from the enlarged half-width of single peak fits (Supplemental Material [37]). Although the data suggest a reentrant tetragonal phase and vanishing lattice orthorhombicity at low temperature, the presence of weak collinear AF order seen by neutron scattering [Figs. 2(c) and 2(d)] indicates that the AF-ordered parts of the sample should still have orthorhombic lattice distortion [19,22]. Figures 3(c) and 3(d) show temperature dependence of the longitudinal scans along the $[H, 0, 0]$ direction for the $x = 0.29$ and 0.31 samples, respectively. While the lattice distortion in the $x = 0.29$ sample behaves similarly to that of the $x = 0.28$ crystal, there are no observable lattice distortions in the probed temperature range for the $x = 0.31$ sample.

To further test the nature of the magnetic-ordered state in $BaFe_2(As_{1-x}P_x)_2$, we have carried out ^{31}P NMR measurements under an 8-T c-axis-aligned magnetic field (Supplemental Material [37]). Figure 4(a) shows the temperature dependence of the integrated spectral weight of the paramagnetic signal, normalized by the Boltzmann factor, for single crystals with $x = 0.25$ and 0.29. For $x = 0.25$, the paramagnetic spectral weight starts to drop below 60 K and reaches zero at 40 K, suggesting a fully ordered magnetic state below 40 K. For $x = 0.29$, the paramagnetic to AF transition becomes much broader, and the magnetic-ordered phase is estimated to be about 50% at $T_c = 28.5$ K. Upon further cooling, the paramagnetic spectral weight drops dramatically below T_c because of radio frequency screening. We find that the lost NMR spectral weight above T_c is not recovered at other frequencies, suggesting that the magnetic-ordered phase does not take full volume of the sample, similar to the spin-glass state of $Ba(Fe_{1-x}T_x)_2As_2$ [21–23].

Figure 4(b) shows the P-doping dependence of the ordered moment squared M^2 in $BaFe_2(As_{1-x}P_x)_2$ including data from Ref. [34]. While M^2 gradually decreases with increasing x for $x \leq 0.25$, it saturates to $M^2 \approx 0.0025 \mu_B^2$ at temperatures just above T_c for $x = 0.28$ and 0.29 before vanishing abruptly for $x \geq 0.30$. The inset in Fig. 4(b) shows the P-doping dependence of the M^2 above and below T_c near optimal superconductivity. While
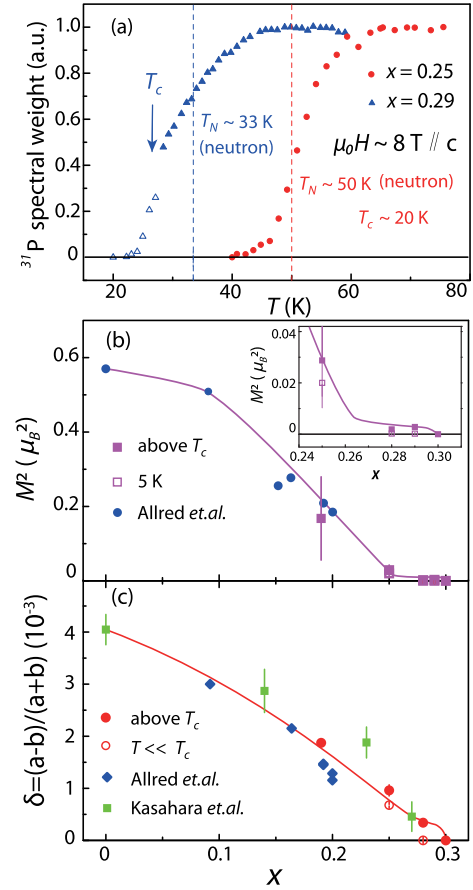

FIG. 4 (color online). (a) Temperature dependence of the paramagnetic spectral weight for $x = 0.25$ and 0.29 samples from NMR measurements. For $x = 0.25$, there are no paramagnetic phases below 40 K, suggesting a fully magnetic-ordered phase. At T_c of the $x = 0.29$ sample, there are still 50% paramagnetic phases suggesting the presence of magnetic signal outside of the radio frequency window of the NMR measurement. The spectral weight loss below T_c is due to superconductivity. The vertical dashed lines mark T_N determined from neutron scattering. (b) The P-doping dependence of M^2 estimated from normalizing the magnetic Bragg intensity to weak nuclear peaks assuming 100% magnetically ordered phase. The blue solid circles are from Ref. [34]. The P-doping levels for different experiments are normalized by their T_N values. The inset shows the expanded view of M^2 around optimal doping above (solid squares) and below (open squares) T_c. (c) The P-doping dependence of δ, where the blue diamonds and green squares are from Refs. [34] and [28], respectively. For samples near optimal superconductivity, the filled and open red circles are δ above and below T_c, respectively.

superconductivity dramatically suppresses M^2, it does not eliminate the ordered moment. Figure 4(c) shows the P-doping dependence of δ in $BaFe_2(As_{1-x}P_x)_2$ below and above T_c. Consistent with the P-doping dependence of M^2 [Fig. 4(b)] and T_N [Fig. 1(c)], we find that δ above T_c approaches $\sim 3 \times 10^{-4}$ near optimal superconductivity before vanishing at $x \geq 0.3$.

Summarizing the results in Figs. 2–4, we present the refined phase diagram of $BaFe_2(As_{1-x}P_x)_2$ in Fig. 1(c). While the present phase diagram is mostly consistent with the earlier transport and neutron scattering work on the system at low P-doping levels [30,34], we have discovered that the magnetic and structural transitions still occur simultaneously above T_c for x approaching optimal superconductivity, and both order parameters vanish at optimal superconductivity with $x = 0.3$. Since our NMR and TRISP measurements for samples near optimal superconductivity suggests spin-glass-like behavior, we conclude that the static AF order in $BaFe_2(As_{1-x}P_x)_2$ disappears in the weakly first-order fashion near optimal superconductivity. Therefore, AF order in phosphorus-doped iron pnictides coexists and competes with superconductivity near optimal superconductivity, much like the electron-doped iron pnictides with an avoided QCP. From the phase diagrams of hole-doped $Ba_{1-x}A_xFe_2As_2$ [8–11], it appears that a QCP may be avoided there as well.

Note added.—We became aware of a theory preprint predicting the first order AF phase transition in $BaFe_2(As_{1-x}P_x)_2$ after the submission of this Letter [38].

---

[*]gfchen@iphy.ac.cn
[†]pdai@rice.edu

[1] Y. Kamihara, T. Watanabe, M. Hirano, and H. Hosono, J. Am. Chem. Soc. **130**, 3296 (2008).
[2] C. de la Cruz et al., Nature (London) **453**, 899 (2008).
[3] Q. Huang, Y. Qiu, Wei Bao, M. A. Green, J. W. Lynn, Y. C. Gasparovic, T. Wu, G. Wu, and X. H. Chen, Phys. Rev. Lett. **101**, 257003 (2008).
[4] M. G. Kim, R. M. Fernandes, A. Kreyssig, J. W. Kim, A. Thaler, S. L. Bud'ko, P. C. Canfield, R. J. McQueeney, J. Schmalian, and A. I. Goldman, Phys. Rev. B **83**, 134522 (2011).
[5] P. Dai, J. Hu, and E. Dagotto, Nat. Phys. **8**, 709 (2012).
[6] M. Rotter, M. Tegel, and D. Johrendt, Phys. Rev. Lett. **101**, 107006 (2008).
[7] R. Cortes-Gil, D. R. Parker, M. J. Pitcher, J. Hadermann, and S. J. Clarke, Chem. Mater. **22**, 4304 (2010).
[8] S. Avci et al., Phys. Rev. B **85**, 184507 (2012).
[9] S. Avci et al., Nat. Commun. **5**, 3845 (2014).
[10] F. Waβer, A. Schneidewind, Y. Sidis, S. Wurmehl, S. Aswartham, B. Büchner, and M. Braden, Phys. Rev. B **91**, 060505(R) (2015).
[11] A. E. Böhmer, F. Hardy, L. Wang, T. Wolf, P. Schweiss, and C. Meingast, arXiv:1412.7038v2.
[12] P. C. Canfield and S. L. Bud'ko, Annu. Rev. Condens. Matter Phys. **1**, 27 (2010).
[13] I. R. Fisher, L. Degiorgi, and Z.-X. Shen, Rep. Prog. Phys. **74**, 124506 (2011).
[14] C. Bernhard, C. N. Wang, L. Nuccio, L. Schulz, O. Zaharko, J. Larsen, C. Aristizabal, M. Willis, A. J. Drew, G. D. Varma, T. Wolf, and C. Niedermayer, Phys. Rev. B **86**, 184509 (2012).
[15] F. L. Ning, K. Ahilan, T. Imai, A. S. Sefat, M. A. McGuire, B. C. Sales, D. Mandrus, P. Cheng, B. Shen, and H.-H. Wen, Phys. Rev. Lett. **104**, 037001 (2010).
[16] R. Zhou, Z. Li, J. Yang, D. L. Sun, C. T. Lin, and G.-Q. Zheng, Nat. Commun. **4**, 2265 (2013).
[17] A. P. Dioguardi et al., Phys. Rev. Lett. **111**, 207201 (2013).
[18] C. Lester, J.-H. Chu, J. G. Analytis, S. C. Capelli, A. S. Erickson, C. L. Condron, M. F. Toney, I. R. Fisher, and S. M. Hayden, Phys. Rev. B **79**, 144523 (2009).
[19] S. Nandi et al., Phys. Rev. Lett. **104**, 057006 (2010).
[20] D. K. Pratt et al., Phys. Rev. Lett. **106**, 257001 (2011).
[21] H. Luo et al., Phys. Rev. Lett. **108**, 247002 (2012).
[22] X. Y. Lu et al., Phys. Rev. Lett. **110**, 257001 (2013).
[23] X. Y. Lu et al., Phys. Rev. B **90**, 024509 (2014).
[24] E. Abrahams and Q. Si, J. Phys. Condens. Matter **23**, 223201 (2011).
[25] S. Jiang, C. Wang, Z. Ren, Y. Luo, G. Cao, and Z.-A. Xu, J. Phys. Condens. Matter **21**, 382203 (2009).
[26] H. Shishido et al., Phys. Rev. Lett. **104**, 057008 (2010).
[27] C. J. van der Beek, M. Konczykowski, S. Kasahara, T. Terashima, R. Okazaki, T. Shibauchi, and Y. Matsuda, Phys. Rev. Lett. **105**, 267002 (2010).
[28] S. Kasahara, T. Shibauchi, K. Hashimoto, K. Ikada, S. Tonegawa, R. Okazaki, H. Shishido, H. Ikeda, H. Takeya, K. Hirata, T. Terashima, and Y. Matsuda, Phys. Rev. B **81**, 184519 (2010).
[29] K. Hashimoto et al., Science **336**, 1554 (2012).
[30] T. Shibauchi, A. Carrington, and Y. Matsuda, Annu. Rev. Condens. Matter Phys. **5**, 113 (2014).
[31] P. Walmsley et al., Phys. Rev. Lett. **110**, 257002 (2013).
[32] J. G. Analytis, H.-H. Kuo, R. D. McDonald, M. Wartenbe, P. M. C. Rourke, N. E. Hussey, and I. R. Fisher, Nat. Phys. **10**, 194 (2014).
[33] Y. Nakai, T. Iye, S. Kitagawa, K. Ishida, H. Ikeda, S. Kasahara, H. Shishido, T. Shibauchi, Y. Matsuda, and T. Terashima, Phys. Rev. Lett. **105**, 107003 (2010).
[34] J. M. Allred et al., Phys. Rev. B **90**, 104513 (2014).
[35] M. Nakajima, S. Uchida, K. Kihou, C. H. Lee, A. Iyo, and H. Eisaki, J. Phys. Soc. Jpn. **81**, 104710 (2012).
[36] T. Keller, K. Habicht, H. Klann, M. Ohl, H. Schneier, and B. Keimer, Appl. Phys. A **74**, s332 (2002).
[37] See the Supplemental Material at http://link.aps.org/supplemental/10.1103/PhysRevLett.114.157002 for a detailed discussion on the experimental setup and additional data.
[38] D. Chowdhury, J. Orenstein, S. Sachdev, and T. Senthil, arXiv:1502.04122.